400 Hz Volume Rate Swept-Source Optical Coherence Tomography at 1060 nm Using a KTN Deflector

Alejandro Martínez Jiménez, Sacha Grelet, Veronika Tsatourian, Patrick Bowen Montague, Adrian Bradu, and Adrian Podoleanu

***Abstract*— In this Letter, a swept-source optical coherence tomography (SS-OCT) instrument employing an innovative scanning protocol for high-speed volumetric rate imaging is demonstrated. The optical source is a tunable laser based on a supercontinuum source pumped with femtosecond pulses, followed by a time-stretched delay fiber. The instrument is equipped with an ultra-fast lateral scanner, based on a KTN crystal, driven at 100 kHz. The letter proves the utility of combining an ultra-fast lateral scanner with an ultra-fast swept laser to provide A-scans at a repetition rate of 40 MHz and an unprecedented 3D-OCT volume acquisition rate of 400 Hz.**

***Index Terms*— OCT, electro-optic modulator, fast imaging, swept source.**

I. Introduction

IN OPTICAL coherence tomography (OCT), the speed of operation is determined by how fast data for axial reflectivity profiles (A-scans/s) are produced. The swept-source (SS) principle allowed an increase in the A-scan rate from a few Hz to hundreds of MHz [1]. For N_x pixels along the fast direction of lateral scanning with a sweeping rate of f, the line rate of the fast (line) scanner is f/N_x. Therefore, with a sweeping rate f of tens of MHz, and a need to have a few hundred N_x points laterally in the image, the lateral scanning rate must exceed tens of kHz. So far, in scanning OCT systems galvanometer-scanners are typically used. For faster speeds, resonant scanners have been harnessed, but they are only available up to a few tens of kHz. In a previous report using a frequency domain mode locked laser (FDML), a resonant scanner was employed [2], enabling volume rates up to 192.5 Hz. Alternatively, full-field swept source OCT configurations could be used to increase the volume rate without need of scanners, shifting the speed limitation to the camera sensor, leading to a 116 Hz volume rate [3]. To make use of the increase in the tuning speed, requires further progress in the deflector technology for lateral scanning. If a multi-MHz swept-source is paired with a galvo or resonant scanner, data will be oversampled along the fast-scanning direction. For larger sweeping frequencies, lateral scanning faster than that provided by resonant scanners is needed. A $KTa_{1-x}Nb_xO_3$ (KTN), crystal-based optical deflector is capable of an order of magnitude faster scanning than resonant scanners. KTN as a sample beam deflector has already been reported in a time domain OCT system [4]. Its fast operation was also employed in a spectral filter to tune the output wavelength in a swept source [5]. In this letter, the tuning rate of the SS employed is $f = 40$ MHz. Therefore, an ultrafast deflector based on a KTN crystal driven by a 100 kHz sinusoidal waveform was utilized. As a result, during each half period of the sinusoidal driving signal applied to the KTN crystal, each fast line (T-scan) contains $N_x = 200$ points. To the best of our knowledge, this is the first report of a KTN scanner being used for sample beam scanning in a SS-OCT system. The swept-source utilized is based on the time-stretch principle, which uses a controlled amount of chromatic dispersion to enlarge a short broadband pulse, to a desired duration. Due to the different speeds at which different wavelengths travel through a dispersive element, sweeping in time is achieved without any active tuning. Thus, the repetition of sweeping events f, is defined by the repetition rate of pulses launched into the dispersive element.

Since the first report on time-stretch based SS-OCT by Moon et al. [6] at 5 MHz, other research groups reported increased sweeping rates using different techniques achieving up to 400 MHz [1]. Most recent reports in time-stretch swept sources have been produced in the telecommunication bandwidth due to the low losses of dispersion compensating fiber used for time-stretching. Here we present a system operating at a more amenable wavelength for biomedical imaging applications, of 1060 nm [7].

II. Methods

A schematic diagram of the SS-OCT instrument is shown in Fig. 1, consisting of an ultrafast swept-source, interferometer and signal processing block. The SS employed here is operating at 40 MHz providing an average optical power

Manuscript received 9 June 2022; revised 8 August 2022; accepted 29 September 2022. Date of publication 4 October 2022; date of current version 14 October 2022. The work of Alejandro Martínez Jiménez, Sacha Grelet, Patrick Bowen Montague, Adrian Bradu, and Adrian Podoleanu was supported by the Marie Curie Training International Training Network (ITN) through the European Commission (EC) under Grant NETLAS-860807. The work of Veronika Tsatourian and Adrian Podoleanu was supported by the University College of London (UCL) Institute of Ophtalmology–Moorfields Eye Hospital London under Grant BRC003. *(Corresponding author: Alejandro Martínez Jiménez.)*

Alejandro Martínez Jiménez, Veronika Tsatourian, Adrian Bradu, and Adrian Podoleanu are with the School of Physical Sciences, University of Kent, CT2 7NZ Canterbury, U.K. (e-mail: alejandromarjim@gmail.com).

Sacha Grelet and Patrick Bowen Montague are with NKT Photonics, 3460 Birkerød, Denmark.

Color versions of one or more figures in this letter are available at https://doi.org/10.1109/LPT.2022.3212015.

Digital Object Identifier 10.1109/LPT.2022.3212015

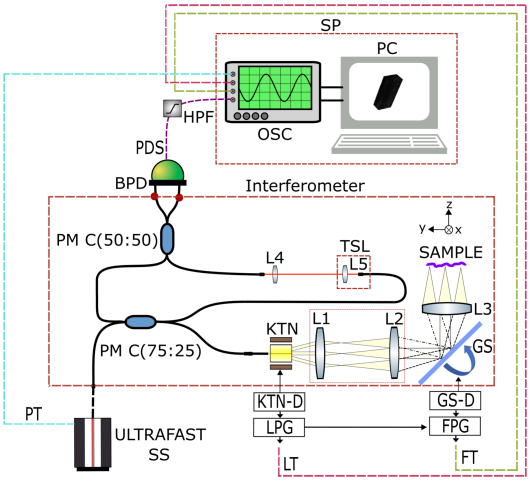

Fig. 1. **Experimental set-up.** SS: swept source; Interferometer (KTN: beam deflector using a KTN crystal, GS: galvanometer scanner, PM C: polarization maintaining couplers, TSL: translation stage launcher); SP: signal processing block (BPD: balanced photodetector, PDS: Photodetected signal, HPF: High pass filter, OSC: oscilloscope, PC: Personal computer); Triggers (LT: line, FT: frame, PT: Optical pulse); Pulse generators (LPG: line, FPG: frame); Drivers (KTN-D: KTN, GS-D: galvanometer scanner). Lenses: L1, L2, L3, L4 and L5 of focal lengths 3 cm, 7.5 cm, 4.5 cm, 1.5 cm and 1.5 cm respectively.

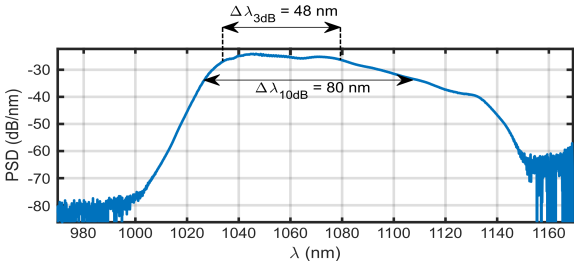

Fig. 2. **Output spectrum** of the supercontinuum time-stretched swept source used in this work.

of 20 mW. The spectrum is centered at 1060 nm and has 48 nm and 80 nm bandwidths at 3 dB and 10 dB respectively, as shown in Fig. 2. The SS design, based on supercontinuum generation followed by a time-stretch stage, is described in detail in [8], with the difference that a 40 MHz seed laser (Origami O10-LP) instead of 80 MHz was used here, with all other seed parameters the same. The supercontinuum is generated in a polarization maintaining (PM) all-normal dispersion fiber (NL-1050-NEG-1-PM by NKT Photonics) and the pulses are stretched using 2.8 km of single mode fiber (980-XP by Nufern). The supercontinuum spectrum is generated by a coherent broadening mechanism [9]. As a consequence, the relative intensity noise of less than 1% is determined by the noise of the pump laser. Pulses of 1 ps duration are stretched up to 12 ns.

The interferometer employs two fiber-based couplers of 25/75 and 50/50 coupling ratios and, 25% of the optical power is guided towards the sample via two lateral scanning devices: a KTN deflector (KTN by NTT Advanced Technology Corporation) for fast line scanning; and a galvanometer scanner (6210H by Cambridge Technology) for frame scanning. The deflection angle of the KTN scanner is proportional to the voltage applied by a high voltage KTN driver (KPS1001CH-00 by NTT Advanced Technology Corporation). The maximum deflection angle is given by the 200 V applied to the crystal. This is fundamentally limited by the thickness of the crystal block [10]. Due to the dependence of deflection angle on the polarization state, the KTN crystal is coupled to a suitably oriented PM fiber by the manufacturer. Therefore, the two couplers in Fig. 1 are also made of PM fiber (PANDA PM980 XP by Nufern). This reduces the losses between the interferometer and the KTN output, however the captured light back from the sample may be affected by the polarisation properties of the sample. The beam shape distortion inside the KTN crystal is compensated by a cylindrical concave lens that reduces the astigmatism and produces a round beam of 1 mm diameter. In order to improve the transversal resolution, the beam is enlarged using a telescope made of two achromatic lenses of 30 mm and 75 mm focal length in the telescope. Finally a 45 mm focal length lens is used to focus the fan of rays onto the sample.

The output optical signal was collected with a 23 GHz bandwidth balanced photodetector (BPR-23-M by Optilab) producing a photodetected signal (PDS), digitized by a 20 GHz bandwidth oscilloscope (Wavemaster 820Zi-b by Lecroy Teledyne). Pulsations given by the pulse repetition rate of the swept source at 40 MHz were eliminated by a 300 MHz high pass filter. The oscilloscope data was collected at 40 GS/s and transferred to a PC for processing.

A common issue in SS-OCT is that, due to nonlinear tuning and dispersion in the interferometer, the PDS is usually chirped in wavenumber. Therefore, different methods, such as phase calibration dispersion compensation (PCDC) and Complex Master Slave (CMS) signal processing [11] have been developed. For its ability to deliver *en-face* views without the need to slice the volume of data, the CMS method was chosen here. For calibration purposes, a flat mirror as a sample was used in the set-up in Fig. 1, and the PDS was acquired for a time duration equal to that of a single sweep of the laser across its spectral range, as shown in Fig. 3(a). This represents the spectrum at the interferometer output. By actuating on the translation stage launcher, 30 such spectra were acquired for 30 values of the optical path difference (OPD) between the interferometer arms, equidistantly separated by 5 μm. Using these experimentally collected spectra, the calibration functions g and h, describing the nonlinearity in the tuning and the unbalanced dispersion between the arms of the interferometer, are presented respectively. The values for g and h were calculated using the procedure described in [12]. Subsequently, the two functions g and h, shown in Fig. 3(b), were employed to theoretically infer interferometric signals (masks). By multiplying the masks with the PDS for each sweep, (corresponding to each lateral pixel acquired while performing the lateral scanning over the sample) cross-sectional and *en-face* images are produced. To implement the protocol used in [12], a MATLAB based software has been developed.

III. Results

Fig. 3 illustrates the depth resolution capabilities of the proposed instrument. The axial resolution is evaluated as $\delta z = 10$ μm calculated for a 48 nm Gaussian shape, due

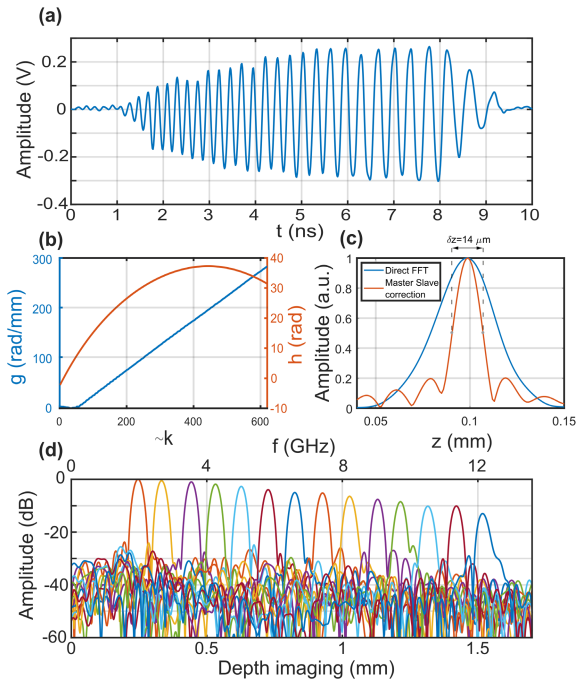

Fig. 3. **Calibration:** (a) Photodetected signal corresponding to a sweep. (b) g and h calibration functions obtained by CMS. (c) Comparison between FFT of uncorrected photodetected signal (blue) and corrected by CMS (red). (d) A-Scans obtained by CMS at 14 different OPD values.

to the spectrum shape of the booster. Furthermore, the A-scan peaks in the Fig. 3(d) display constant width across the entire axial range with a sensitivity profile decay rate of 8 dB/mm. An attenuation of 6 dB is obtained for an axial range Δz of 0.61 mm in depth along coordinate Z. Near OPD $= 0$, a signal to noise ratio of ~ 45 dB is achieved. Fig. 3(b) also shows that the chirp in the channeled spectrum modulation is mainly created by the dispersion, as the g function is almost linear. Since the sensitivity is currently insufficient to produce images from biological scattering samples, instead the imaging capability is demonstrated using the topography of a coin.

To perform imaging, the KTN driver delivered 200 V amplitude sinusoidal driving voltage at 100 kHz, producing a full detection angle of 124 mrad that covered 2.95 mm along X-direction. The raster formed by the two scanners comprises N_y lines, with each line consisting of N_x points. The lateral resolution, measured using an USAF target, is 23 µm in the x-direction and 18 µm along the y-direction. The different resolution along the x and y axes is expected due to imperfect compensation of the beam astigmatism introduced by the KTN crystal, only partially reduced by the cylindrical lens installed by the manufacturer at the output of the KTN crystal. These lateral resolutions are similar to those previously reported on using a KTN crystal for sample beam scanning [4]. The image is limited along X due to the limited size created by the KTN deflector, hence to cover a larger area we increased the image size along Y to 6.6 mm by driving the frame galvoscanner with an amplitude of 2.5 Vpp. By driving the galvanometer-scanner with a sawtooth signal at 400 Hz gives a number of $N_y =$ 250 lines in the *en-face* image. In the images presented in Fig. 4-6 only half period of the signal driving the KTN is used for simplicity. If both lateral scanning directions of the

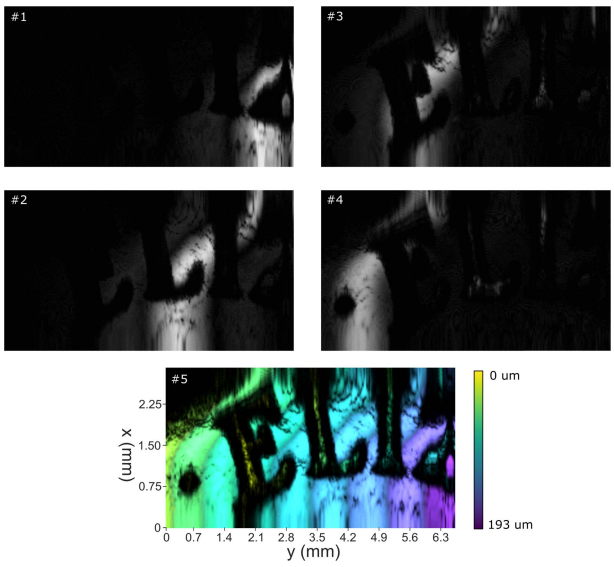

Fig. 4. **Raw *en-face* OCT images.** (1-4) OCT images from different Z coordinate values separated by 40 µm along Z direction. (5) Superposition of 10 images separated by 10 µm along Z-direction, where the height position along Z is colorcoded. Black color means no signal.

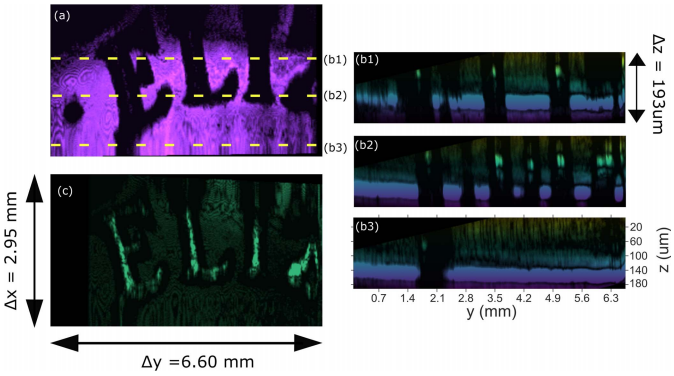

Fig. 5. **Tilt corrected OCT images**. (a) *En-face* image of the bottom of the letters. (b1-3) B-scans at lateral positions as indicated by dashed yellow lines in (a). (c) *En-face* image of the top of the letters.

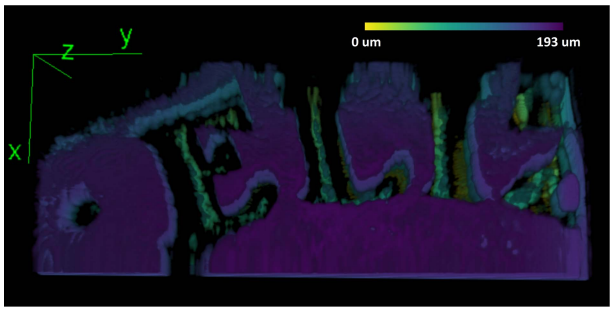

Fig. 6. **Topographical representation of a 3D volume** generated in a raster at 400 Hz from the coin, where the colorbar is used to illustrate the Z coordinate.

KTN scanner would be used to assemble an *en-face* image, for the same number of lines, the frame rate could be doubled.

Fig. 4 shows *en-face* OCT images of a coin from 4 positions z separated by 40 µm. The coin was slightly tilted, and therefore the narrow axial resolution led to fragmented *en-face* OCT images. The 5th image underneath represents a summation of 10 *en-face* images separated 10 µm into a single projection, where the height in Z of each image was colorcoded. The thickness of the bright patch in the *en-face* OCT images

represents a projection of the axial resolution interval along the tilted surface of the coin. To widen the bright patch, the tilt of the coin in the volume of data acquired has been compensated by software means and two such *en-face* cuts, corrected for tilt, corresponding to the Z-position of the coin base (a) and the top of the letters (c) are shown in Fig. 5. Fig. 5(b1–b3) shows three B-scan OCT images. These are perpendicular to the *en-face* OCT image in Fig. 5(a) and oriented along the dashed lines superposed on the same image. The images in Fig. 4–5 confirm that the axial range is sufficient to cover the tilt of the coin and the height of the letters on the coin. Topography of the 3D volume generated is shown in Fig. 6. Due to the sinusoidal shape of the signal driving the KTN deflector, the images present a nonlinear variation of pixel size along the x-line in the raster. Therefore, margins were cropped to eliminate the regions of flyback, and afterwards corrected along the x-direction via linear interpolation in postprocessing. Considering the numerical values for the axial range and axial resolution evaluated above, a number of points $N_z = \Delta z/\delta z = 53$ along the depth coordinate is obtained. Therefore, using one half of KTN ramp, the displayed volume contains $200 \times 250 \times 53$ voxels.

IV. Conclusion

This work responds to the progress in the high sweeping speed of modern tuning lasers. Galvanometer and resonant scanners are widely used in OCT instruments, however, when paired with a fast sweeping optical source, the distance between successive lateral pixels becomes smaller than the optical transversal resolution, which effectively turns into data oversampling with no effective increase in the volume acquisition rate. The effective scanning procedure using a fast KTN-based scanner shown in this report demonstrated a volume production rate of up to 400 Hz, which is superior to other reported with OCT scanning systems operating in the 1 μm band [2]. In the case of moving targets, the high-volume rate secures less distortion due to movement. This could benefit several applications such as: phase-sensitive OCT, surgery guidance, and 4D-OCT [13]. However, increasing the sweeping speed comes at the expense of limited sensitivity. With a duty cycle $\sim$ 50%, operating at 40 MHz repetition rate, this corresponds to an equivalent sweeping at 80 MHz with 100 % duty cycle. According to the estimated formula for variation of sensitivity with the sweeping speed in Boer et al. [14], a 30 dB reduction is due to the increase in the sweeping rate from 1 MHz to 100 MHz. This comparison does not yet consider larger noise levels owing to increase in the electronic bandwidth by 80 times when the sweeping rate is increased from 1 to 80 MHz. For instance, in a previous report Klein et al. [13], obtained a sensitivity of 90 dB at a sweeping rate of 1 MHz. Therefore, by taking into account two corrections applied to a 90 dB sensitivity considered as norm: (i) suggested in [14] and (ii) due to enlarged noise bandwidth may lead to a much lower value, closer to that reported here. A modest improvement in sensitivity is possible by reducing the ratio of the first coupler accompanied by a proportional increase in the optical power of the source for the same safety power limit delivered to the sample. Care was taken in assembling a low noise swept source, compared with classical supercontinuum sources based on solitons. The coherent supercontinuum mechanism used in this report led to a reduced excess photon noise given by the relative intensity noise. Despite this, it was found that the balanced detection scheme was unable to fully remove deterministic noise in the range of $3-5$ GHz which will require further investigations. Another limitation of the instrument reported is given by the data acquisition. Although digital sampling acquisition is able to cope with tens of GHz, such high electrical bandwidths when combined with a dynamic range of 12 bits leads to a large volume of data. Due to the limited transfer speed and data processing time required, this prevents real-time delivery of images. Improvements in reducing deterministic noise of fast sweeping sources accompanied by a better trade-off between sweeping time and volume acquisition time could enable system architecture as described here, to benefit both biomedical and industrial applications.

Acknowledgment

Adrian Bradu and Adrian Podoleanu are coinventors on patents in the name of the University of Kent.

References

[1] D. Huang, F. Li, Z. He, Z. Cheng, C. Shang, and P. K. A. Wai, "400 MHz ultrafast optical coherence tomography," *Opt. Lett.*, vol. 45, no. 24, pp. 6675–6678, Dec. 2020.

[2] J. P. Kolb, T. Klein, W. Wieser, W. Draxinger, and R. Huber, "Full volumetric video rate OCT of the posterior eye with up to 195.2 volumes/s," *Proc. SPIE*, vol. 9312, pp. 11–17, Mar. 2015.

[3] E. Auksorius et al., "In vivo imaging of the human cornea with high-speed and high-resolution Fourier-domain full-field optical coherence tomography," *Biomed. Opt. Exp.*, vol. 11, no. 5, pp. 2849–2865, 2020.

[4] M. Ohmi, Y. Shinya, J. Miyazu, S. Toyoda, and T. Sakamoto, "High-speed time-domain En face optical coherence tomography system using KTN optical beam deflector," *Opt. Photon. J.*, vol. 9, no. 5, pp. 53–59, 2019.

[5] Y. Okabe et al., "200 kHz swept light source equipped with KTN deflector for optical coherence tomography," *Electron. Lett.*, vol. 48, no. 4, pp. 201–202, 2012.

[6] S. Moon and D. Y. Kim, "Ultra-high-speed optical coherence tomography with a stretched pulse supercontinuum source," *Opt. Exp.*, vol. 14, no. 24, pp. 11575–11584, Nov. 2006.

[7] X. Wei, A. K. S. Lau, Y. Xu, K. K. Tsia, and K. K. Y. Wong, "28 MHz swept source at 1.0 μm for ultrafast quantitative phase imaging," *Biomed. Opt. Exp.*, vol. 6, no. 10, pp. 3855–3864, Nov. 2015.

[8] S. Grelet, P. Bowen, P. M. Moselund, and A. Podoleanu, "80 MHz swept source operating at 1060 nm based on all- normal-dispersion supercontinuum generation for ultrahigh-speed optical coherence tomography," in *Proc. Eur. Conf. Biomed. Opt.* Rochester, NY, USA: Optical Society of America, Jun. 2021, p. ETu3D5.

[9] E. Genier et al., "Ultra-flat, low-noise, and linearly polarized fiber supercontinuum source covering 670-1390 nm," *Opt. Lett.*, vol. 47, no. 8, pp. 1820–1823, Mar. 2022.

[10] T. Imai, M. Ueno, Y. Sasaki, and T. Sakamoto, "Analyses of optical rays in KTN optical beam deflectors for device design," *Appl. Opt.*, vol. 56, no. 25, pp. 7277–7285, 2017.

[11] S. Rivet, M. Maria, A. Bradu, T. Feuchter, L. Leick, and A. Podoleanu, "Complex master slave interferometry," *Opt. Exp.*, vol. 24, no. 3, pp. 2885–2904, Feb. 2016.

[12] A. Bradu et al., "Recovering distance information in spectral domain interferometry," *Sci. Rep.*, vol. 8, no. 1, pp. 1–16, Oct. 2018.

[13] T. Klein, W. Wieser, L. Reznicek, A. Neubauer, A. Kampik, and R. Huber, "Multi-MHz retinal OCT," *Biomed. Opt. Exp.*, vol. 4, pp. 1890–1908, Oct. 2013.

[14] J. F. de Boer, B. Cense, B. H. Park, M. C. Pierce, G. J. Tearney, and B. E. Bouma, "Improved signal-to-noise ratio in spectral-domain compared with time-domain optical coherence tomography," *Opt. Lett.*, vol. 28, no. 21, pp. 2067–2069, 2003.